SPACE TELESCOPE SCIENCE INSTITUTE
Operated for NASA by AURA

Instrument Science Report NICMOS 2009-006

NICMOS Grism Wavelength Calibration

N. Pirzkal, R. Bohlin, D. Thatte
Jun 30, 2009

ABSTRACT

As part of the Cycle 16 NICMOS calibration program, new observations of planetary nebulae were obtained using all three NICMOS grisms (G096, G141, and G206). The aim of these observations was to re-derive the dispersion relations for the grism modes of NICMOS as well as to examine and parametrize any field dependence of the dispersion relation within the field of view of the instrument. In this ISR, we present updated versions of the dispersion relations of the G096, G141, and G206 grisms. While the field dependence is small (1-2% peak to peak variation), we also compute two dimensional polynomial solutions to compute more exact dispersion relations anywhere in the field of view of NICMOS.

Introduction

NICMOS is one of several HST instruments which offers users the opportunity to obtain sensitive slitless spectroscopic observations. Using a combination of three distinct grism elements, low resolution slitless spectroscopy can be obtained in the wavelength range from 0.8 to 2.5 microns using the NIC3 camera.

Because NICMOS does not have internal calibration lamps, a-priori calibration of its spectroscopic mode is required using real observations of known emission line sources.

A dispersion relation for the grism was derived in 1997 following the installation of NICMOS on HST. As part of an effort to obtain a final calibration of the NICMOS spectroscopic mode, two planetary nebulae, VY2-2 and HB12, were observed. These objects have a few bright emission lines in the near-infrared that are clearly separated in NICMOS grism observations.

Data

We obtained these data as part of an effort to re-evaluate the calibration of the NICMOS grisms during Cycle 16. These data we obtained as part of the calibration proposal 11331 (PI: N. Pirzkal). For the purpose of wavelength calibrating the NICMOS grisms, we observed two targets, VY2-2 and HB12, as shown in Table 1.

Table 1: List of wavelength calibration targets for proposal 11331.

	RA	DEC	Observation Date	SIMBAD ID
VY2-2	291.092583	9.899222	2008-04-29	PN G045.4-02.7
HB12	351.561667	58.181667	2008-01-20	PN G111.8-02.8

Both of these targets were placed at 8 different positions on the detector, as shown in Figures 1 and 2. At each of these positions, the target was observed first using the F160W filter to provide a reference position image of the source in the field of view. Immediately following was a series of observations using the G096, G141, and G206 grisms. The individual observation times for each object and filter are listed in Table 2.

Because extraction of slitless spectra requires a wavelength reference point, the position of the object in the field is traditionally used as this reference point. A direct image must be immediately followed by slitless observations in order to ensure that the telescope pointing remains locked on the same guide stars to make sure that there are no additional shifts in positions between the direct and the slitless images.

Proposal 11331 was designed to place each target in each of the four corners of the NIC3 detector in order to maximize the effect of any field dependence/distortion. Targets were also observed nearer to the bottom of the chip in order to detect potential temporal variations as well as measure effect of small scale shifts in the dispersion relation.

Furthermore, since VY2-2 and HB12 observations were taken several months apart, they verify that the system is stable on the time scale of weeks.

Table 2: Filter, sample sequence, and exposure times used for the wavelength calibration targets in proposal 11331.

	Filter	SAMP_SEQ	NSAMP	Exposure Time (s)
VY2-2	F160W	STEP2	9	10.00
	G096	STEP8	13	56.00
	G141	STEP8	13	56.00
	G206	STEP8	13	56.00
HB12	F160W	STEP2	9	10.00
	G096	STEP8	13	56.00
	G141	STEP8	13	56.00
	G206	STEP8	13	56.00

Figure 1: This set of four images shows the four positions on the NICMOS 3 chip where both VY2-2 and HB12 were observed (brightest spectrum in each of the four pointings). Wavelength increases from the right to the left and the second order spectra can be seen when the first order is near the right side. The point-like zeroth order appears when the first order is near the left side.

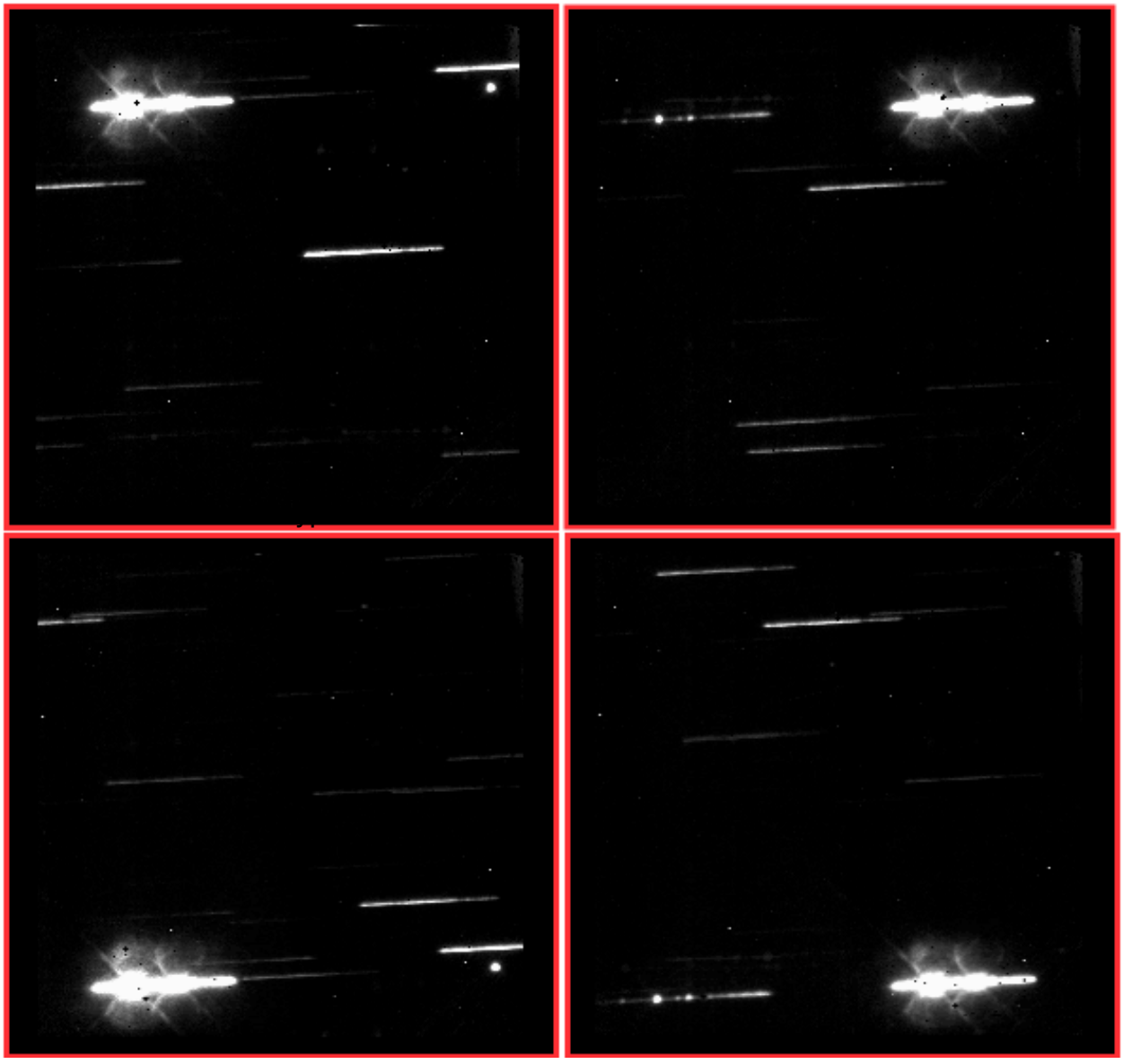

\

Figure 2: Positions at which the sources VY2-2 (red) and HB12 (green) were observed in the NICMOS detector using the F160W, G096, G141, and G206 dispersers.

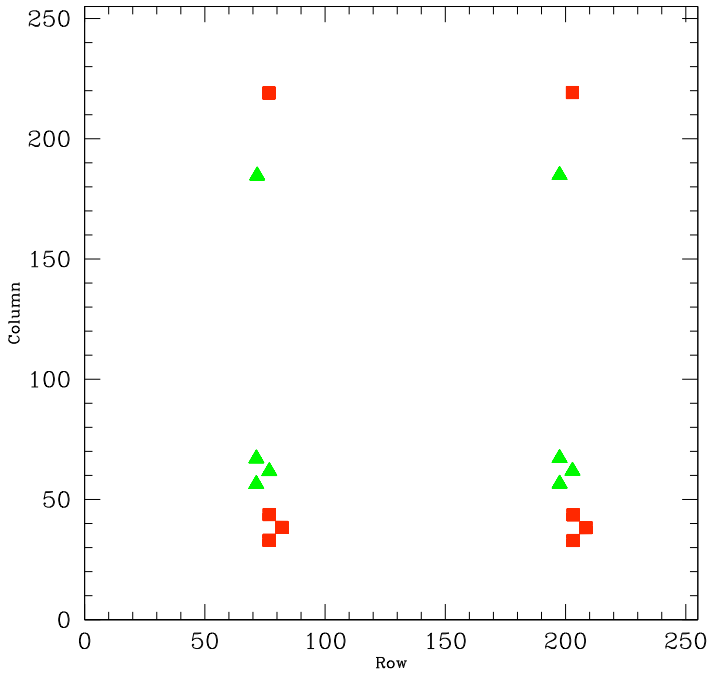

Processing

The data were retrieved from the MAST archive and were automatically reduced using the on-the-fly re-processing (OTFR) of OPUS 2008.1 and version 4.1.1 of CALNICA. The slitless images are fully reduced (bias and dark subtracted) but not flat-fielded while the direct images (F160W) are bias and dark subtracted as well as flat-fielded.

Identifying Emission Lines in the reference spectrum

Ground based observations of HB12 and VY2-2 served as our wavelength reference spectra (Hora 1999). The resolution of these spectra are higher (9Å/element) than those obtained using either of the three NICMOS grisms and some of the emission lines are blended in the NICMOS observations. The reference spectra were therefore first smoothed down to a resolution that is close to that of NICMOS using a 200Å Hanning smoothing window. These are plotted in Figures 3 and 4. The center wavelength of the lines or line blends in the smoothed reference spectra were carefully measured using IRAF and the SPLOT task in the NOAO ONEDSPEC package by fitting a 1D gaussian to each blend and to accurately measure the effective wavelength of each feature. These reference line wavelengths were then converted from air to vaccum. Throughout this ISR, all wavelengths refer to vacuum wavelengths. Both the HB12 and the VY2-2 have identical reference wavelengths. In this ISR, we refer only to the VY2-2 spectum for this reason.

Figure 3: Reference VY2-2 Planetary Nebula spectrum from 0.8 to 1.4 micron (black) and the smoothed version of it (red). Several lines are blended at the NICMOS resolution.

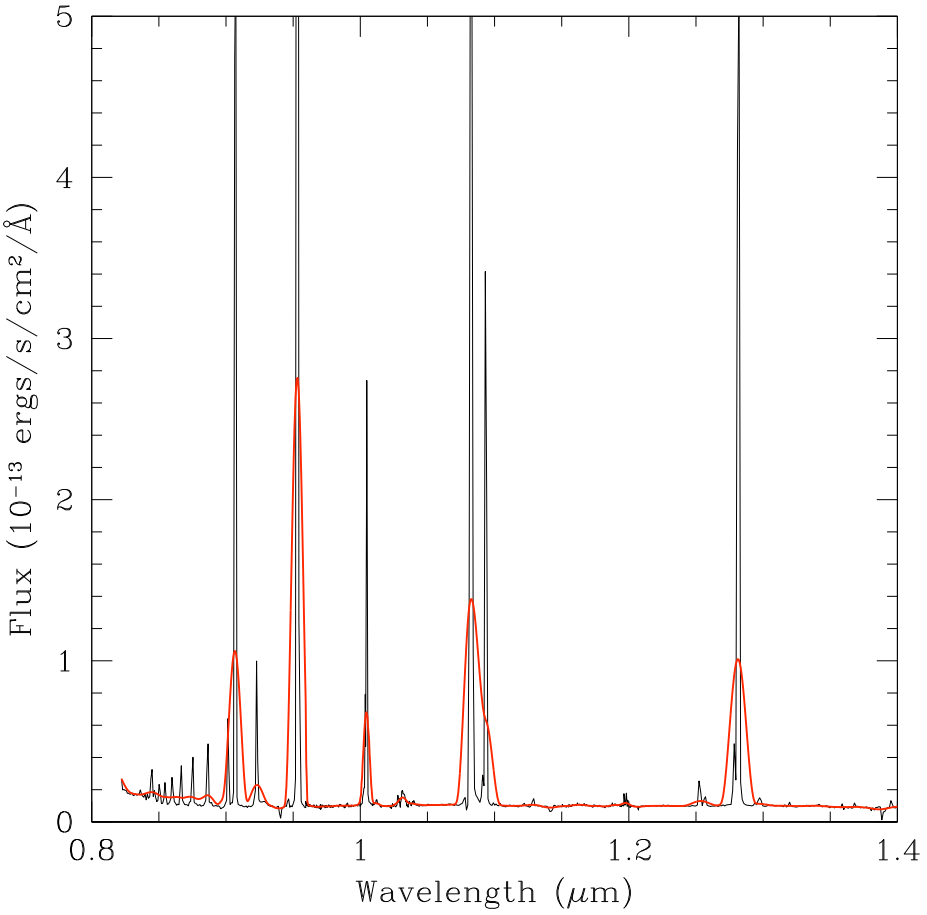

Figure 4: Same as Figure 3 but plotting the wavelength range of 1.4 to 2.2 micron. The missing data from 1.8 to 1.96 microns from this ground-based reference spectrum is due to atmospheric absorption.

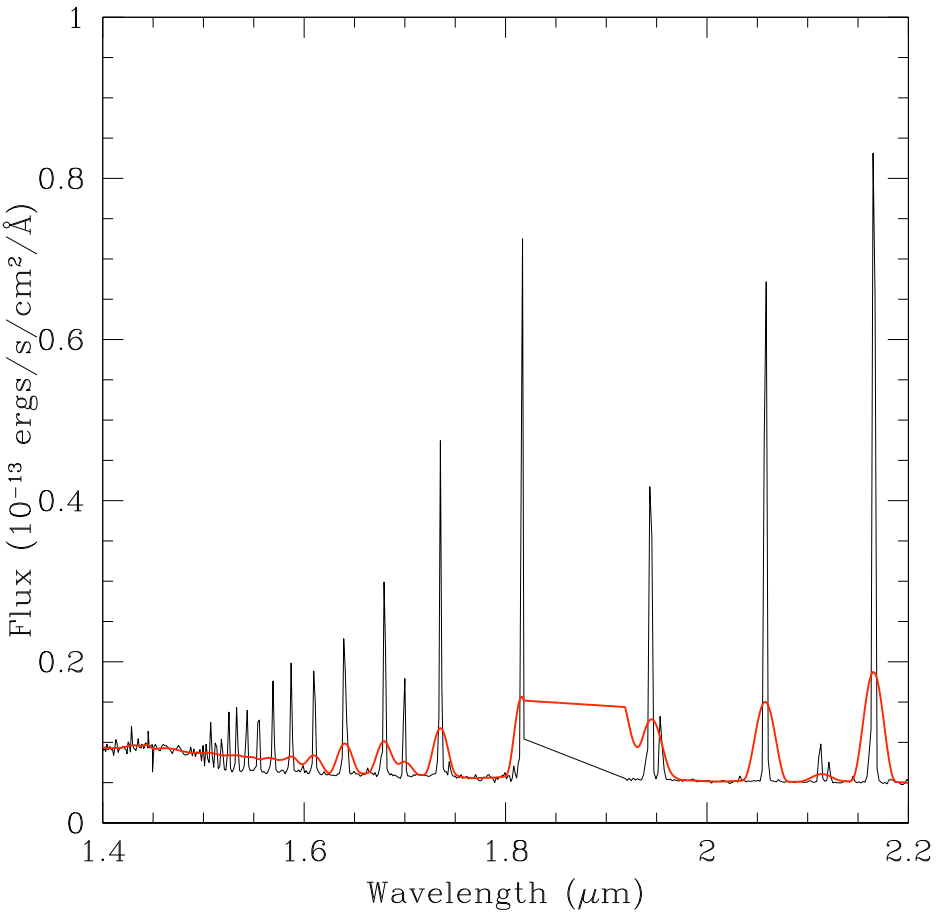

Grism Calibration and Field Dependence

The Spectral Trace

The basic geometry of the NICMOS grism mode is shown in Figure 5. In this figure, we show the known location of a source (red circle) and the trace (thick back line) that is produced once a grism element is inserted into the optical path.

Figure 5: The basic geometry of the NICMOS grism mode.

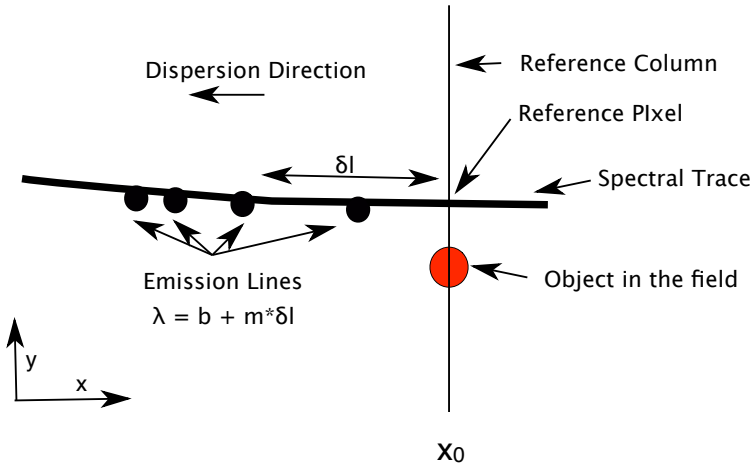

The NICMOS grism dispersion relations are already known to be linear, and the spectral traces are also known to be linear. This greatly simplifies the calibration of this mode. In this ISR, the spectral trace of the grism is parametrized as a polynomial of the form:

(1) $$y = a + b * (x - x_0) + c * (x - x_0)^2$$

where x_0 is the x, or column, position of the reference pixel, i.e. the known x-position of the source in the field of view, as measured using a direct image such as the ones we acquired using the F160W filter.

In the case of NICMOS, the angle of the spectral trace varies slightly every time a grism element is rotated into place. In order to extract NICMOS grism data, the location of the spectrum must first be accurately determined. The latter was done by measuring the positions of emission lines in the 2D grism images directly and by fitting x,y positions to Equation 1. The fact that the NICMOS grism dispersion is well parametrized using a simple linear relation was verified, keeping only the terms a and b in Equation 1. While the slope of the trace can vary slightly each time a grism is used, this effect is small (< 0.4 degree). Both the value as well as the

observed variation in the measured slope of the dispersions for the G096, G141, and G206 grisms are summarized in Table 3.

The vertical offset between the source in the direct image and its corresponding trace in the 2D grism image, as shown in Figure 5, is also known to vary slightly from one observation to the

Table 3: Mean value of the angle between the spectral trace and the horizontal for all 16 HB12 and VY2-2 observations. The standard deviation of the mean (σ) is also shown.

	Slope (degree)	σ
G096	3.05	0.19
G141	0.95	0.20
G206	1.27	0.36

next. Table 4 gives the average y-offset between the source and the spectral trace in pixels, at reference pixel x_0. These offsets are stable both spatially and temporally as the typical RMS is 0.11 pixel for all three grisms.

Table 4: Offset between the source y coordinate and the spectral trace in the grism image for each of the three NICMOS grisms, at the reference pixel x_0 position.

	dy (pixel)	σ
G096	-4.38	0.11
G141	-6.86	0.11
G206	-2.20	0.11

Wavelength Calibration

Along the line, as parametrized by the equation above, a position on the spectral trace can be related to a physical wavelength. For nearly linear dispersions such as the NICMOS grism, a simple polynomial relation is sufficient:

(2)

where λ is the wavelength along the trace of a given pixel that is at a distance of δl pixels away from the reference pixel x_0. This reference pixel is defined as the pixel along the trace which is at the same column position as the object in the direct image, as shown in Figure 5.

$$\lambda = b + m_1 * \delta l$$

Finally, we can account for any field dependence to the dispersion relation (Equation 2) by determining this relation at different locations in the field of view. At each of these location (i.j), we can the derive:

(3)

which is a generalization of Equation 2 where b and m values are computed for a known source position of (i,j) in the detector using:

$$\lambda_{i,j} = b_{i,j} + m_{i,j} * \delta l$$

(4)

$$b_{i,j} = b_0 + b_1 * x + b_2 * y$$

$$m_{i,j} = m_0 + m_1 * x + m_2 * y$$

Identifying Emission Lines in the NICMOS spectra

In order to compute the parameters b and m in Equation 2, we first identified the position of the emission lines in the NICMOS data by producing 1D extracted, but not flux calibrated spectra. These 1D spectra were generated by solving Equation 1 for the position of bright emission features along the trace and by then appropriately row collapsing each spectrum into bins along the actual trace of the spectrum. This was done individually for each of our 16 observations and was necessary since, as we saw, the NICMOS grism spectra are not always projected at exactly the same angle with respect to the horizontal. Non zero values of this dispersion angle mean that one must not simply row collapse the spectra but extract them along the trace. This is similar to what is being done by the extraction software aXe (Kümmel, 2009).

The results of individually extracting each spectrum was the production of eight 1D spectra of HB12 and eight 1D spectra of VY2-2. Examples of these extracted 1D spectra for G096, G141, and G206 are shown in Figures 6, 7, and 8, respectively. The position of individual emission features along the trace of each spectra was measured using SPLOT. For each spectrum, distances along the spectral trace between features and the reference pixel were determined and a reference wavelength was assigned to each feature (as obtained using the ground based reference spectra described above). Figures 6, 7, and 8 show identified lines (dashed lines) and their center wavelengths are labeled.

Figure 6: Extracted 1D spectrum of HB12 as seen using the G096 grism. X-axis shows the distance between a given pixel in the spectrum and the known position of the object measured in the F160W image. Identified lines are shown with dash lines and are labeled with the vacuum wavelengths used in our dispersion solutions. The NICMOS grism dispersion direction is right to left.

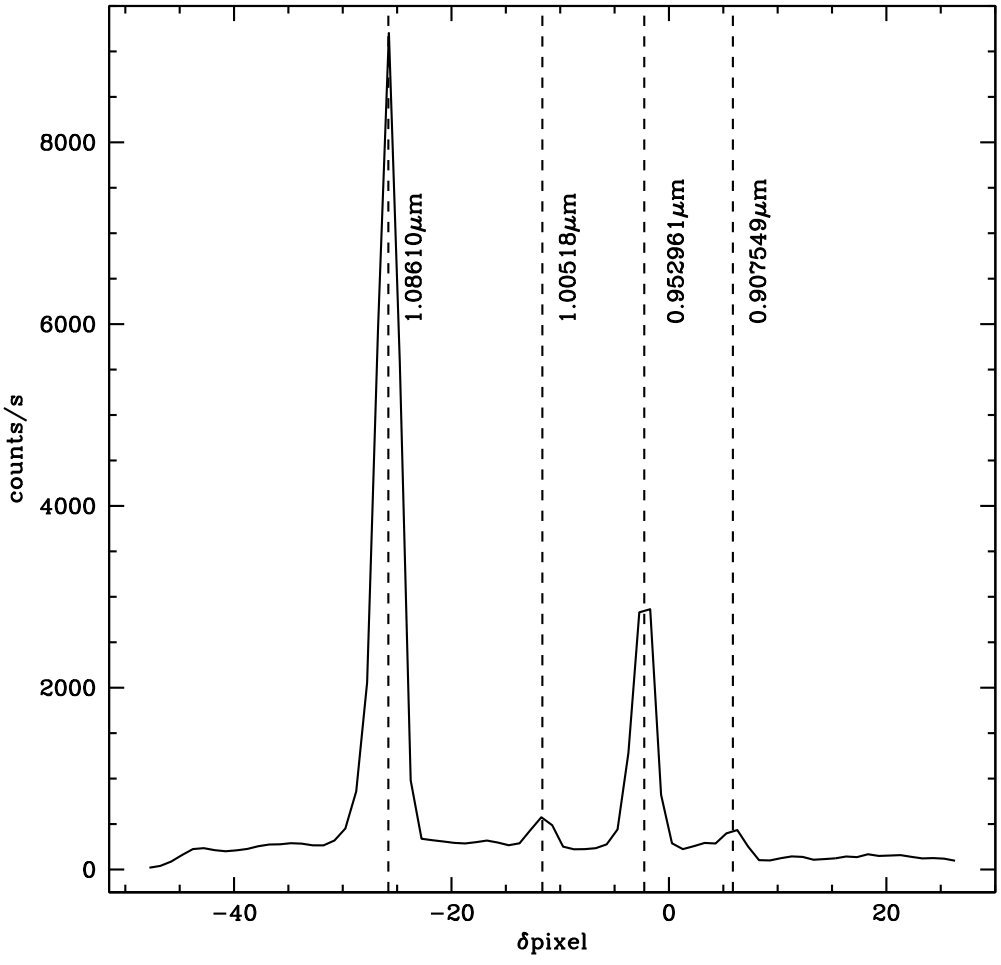

Figure 7: Extracted 1D spectrum of HB12 as seen using the G141 grism. X-axis shows the distance between a given pixel in the spectrum and the known position of the object measured in the F160W image. Identified lines are shown with dash lines and are labeled with the vacuum wavelengths used in our dispersion solutions. The NICMOS grism dispersion direction is right to left.

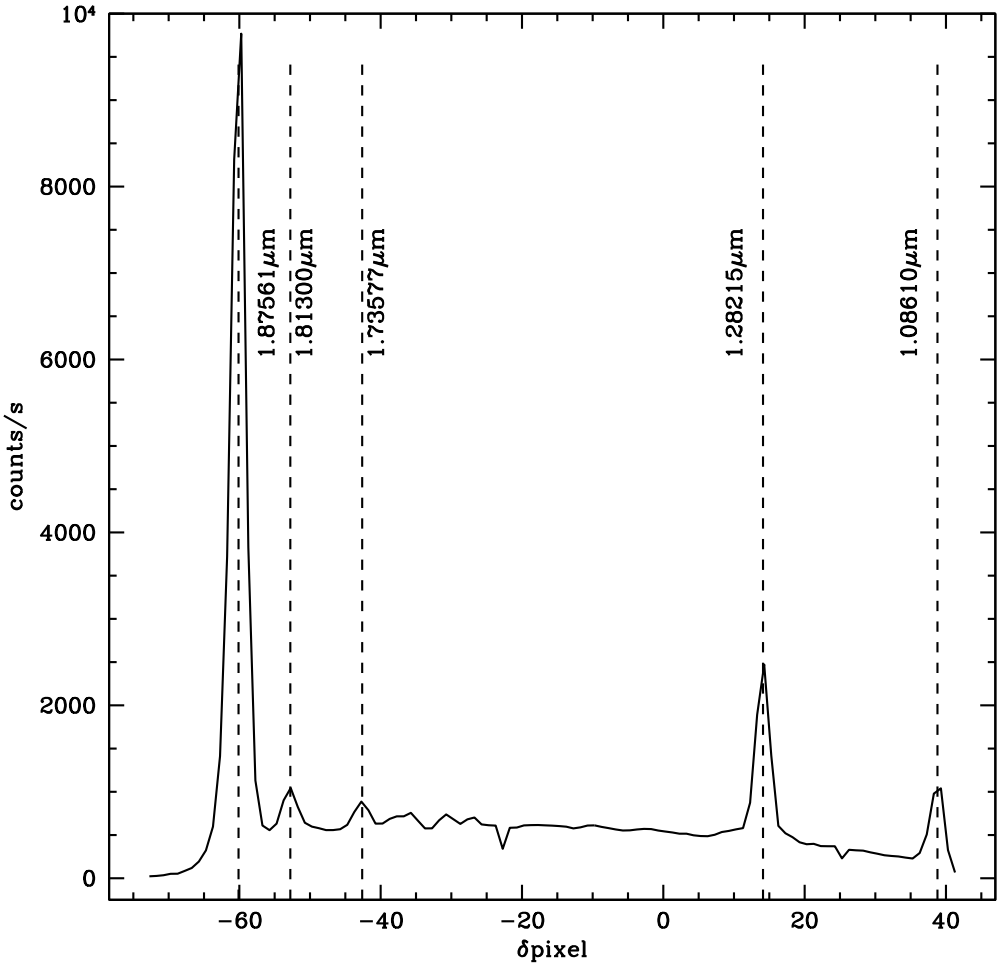

Figure 8: Extracted 1D spectrum of HB12 as seen using the G206 grism. X-axis shows the distance between a given pixel in the spectrum and the known position of the object measured in the F160W image. Identified lines are shown with dash lines and are labeled with the vacuum wavelengths used in our dispersion solutions. The NICMOS grism dispersion direction is right to left.

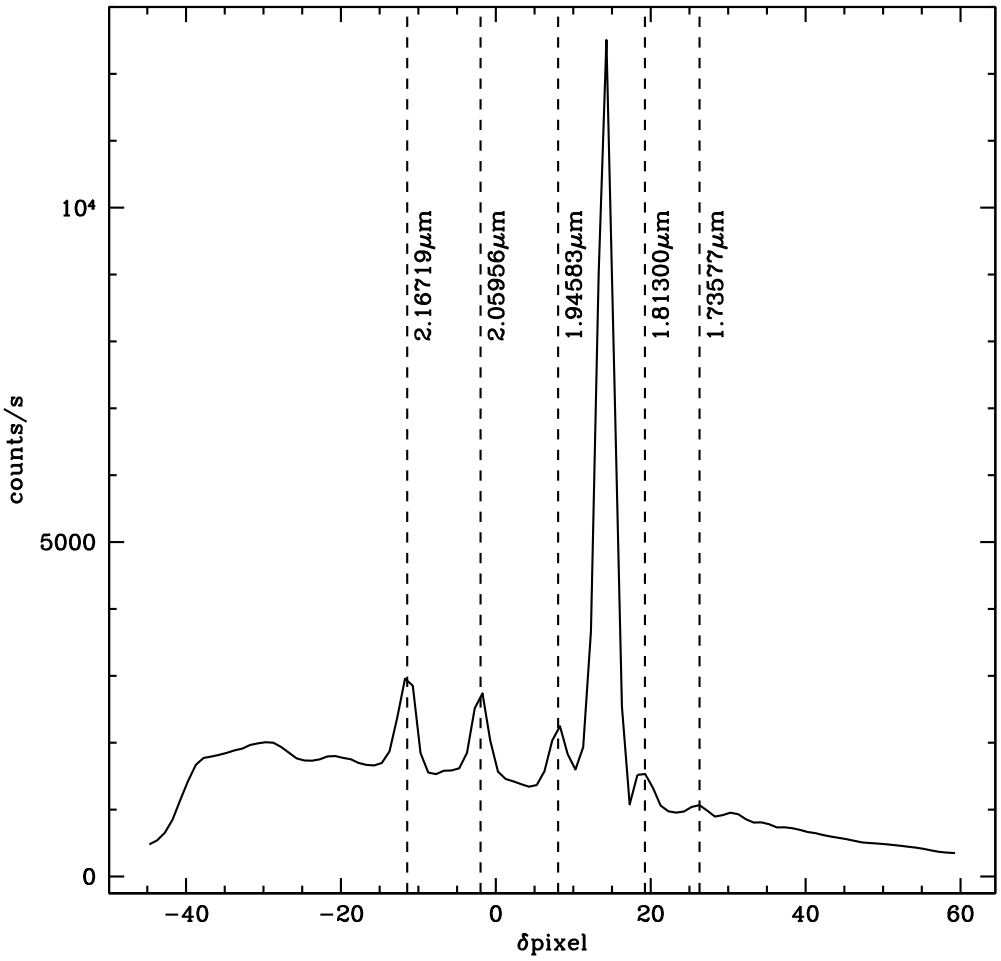

Results:

Having identified emission lines for all three grisms, the coefficients b and m in equation 3 were computed at the 16 independent positions shown in Figure 2. A linear relation is a very good fit to the measured dispersion of all three grisms and the typical RMS between the linear fit at each position and a straight line is on the order of 0.001μm, which is less than a quarter of a width of a pixel along the trace.

The following table lists the average values of the parameters b and m for all three grisms.

The small rms values shown in Table 5 are an indication of the stability of all three grisms, both temporally and physically.

Table 5: Average dispersion coefficients for the G096, G141, and G206 grisms

	b	**m**
G096	0.941676± 0.001142	-0.00562722±0.00002710
G141	1.39722±0.0016694	-0.0079959±0.00001156
G206	2.03855±0.0025908	-0.0114779±0.00011738

Following the methodology outlined above, as summarized by equations 3 and 4, the field dependent polynomial for the b and m coefficients were computed and these are shown in Table 6.

The field dependence of the b and m parameters are small and most applications should not require the use of these field dependent relations. The corner to corner variation in the b and m values for all three grisms are within 1-2%, as shown in Figure 9.

Table 6: Field dependent parameters for the wavelength calibration coefficients of all three grisms. The coefficients of the dispersion relation, as shown in equation 3, can be computed using equation 4 and the values below.

	b_0	b_1	b_2
G096	0.939668	1.489×10^{-5}	-6.28038×10^{-7}
G141	1.39384	2.48266×10^{-5}	-5.77059×10^{-7}
G206	2.03351	3.47129×10^{-5}	2.66593×10^{-6}
	m_0	m_1	m_2
G096	-0.00562402	1.90631×10^{-8}	-6.63082×10^{-8}
G141	-0.00799263	6.28868×10^{-8}	-1.36104×10^{-7}
G206	-0.0114426	-2.71002×10^{-8}	-3.57863×10^{-7}

Time Variation

As mentioned above, the observations of HB12 and VY2-2 were taken nearly three months apart. This gave us a unique opportunity to look for temporal variation of the NICMOS grism dispersion relations.

There is no measurable variation between the two epochs and this ISR reflect this as all the data were combined together to compute a unique set of dispersion relation and a unique set of field dependent dispersion relation. Any time dependence of the NICMOS grism dispersion is small and undetected here and remains significantly smaller than our ability to accurately measure the centroid of lines in the 2D images (to compute the trace of each sprectum) and the centroid of lines in the extracted uncalibrated 1D spectra (to compute the b and m parameters as explained above).

Comparison with previous values

As listed in the NICMOS Instrument Handbook, the previous and updated NICMOS wavelength dispersion solution are shown in the following Table:

Figure 9: Field dependence of the b (left panels) and m (right panels) dispersion parameters. The y axis is percentage change from the position (128,128) on the detector.

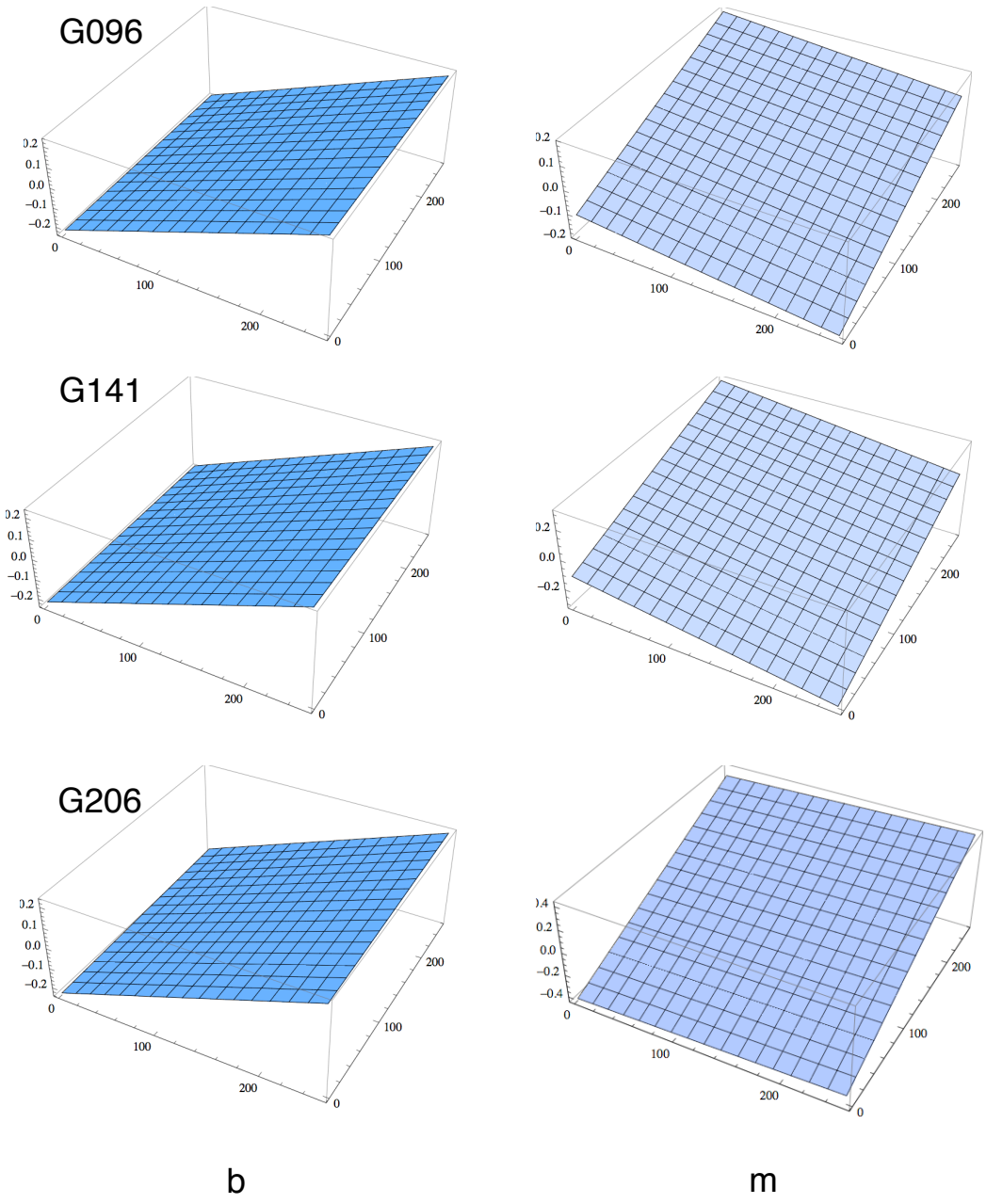

Table 7: New versus Old NICMOS wavelength calibration values. The old values shown here are from the NICMOS Instrument Handbook v. 10.0.

	This Work		Existing Values	
	b	**m**	**m**	**b**
G096	0.941676 ± 0.001142	-0.00562722 ±0.00002710	0.9487	-0.00536
G141	1.39722 ±0.0016694	-0.0079959 ±0.00001156	1.401	-0.007992
G206	2.03855 ±0.0025908	-0.0114779 ±0.00011738	2.045	-0.01152

In order to illustrate the potential gains obtained when calibrating the NICMOS grism spectra using the field dependent quantities listed in Table 5, we show in Figures 10 and 11 extracted and wavelength calibrated spectra of VY2-2 and HB12. There, we visually show the small gain one can obtain when accounting for the field dependence of the NICMOS grisms. As shown in the right most panels, all three grisms show a much tighter agreement between the eight individually extracted spectra of VY2-2 and HB12.

Figure 10: VY2-2 extracted using the field dependent wavelength calibration from this work and extracted using previously published values of m and b. All 8 wavelength calibrated spectra are shown over-plotted.

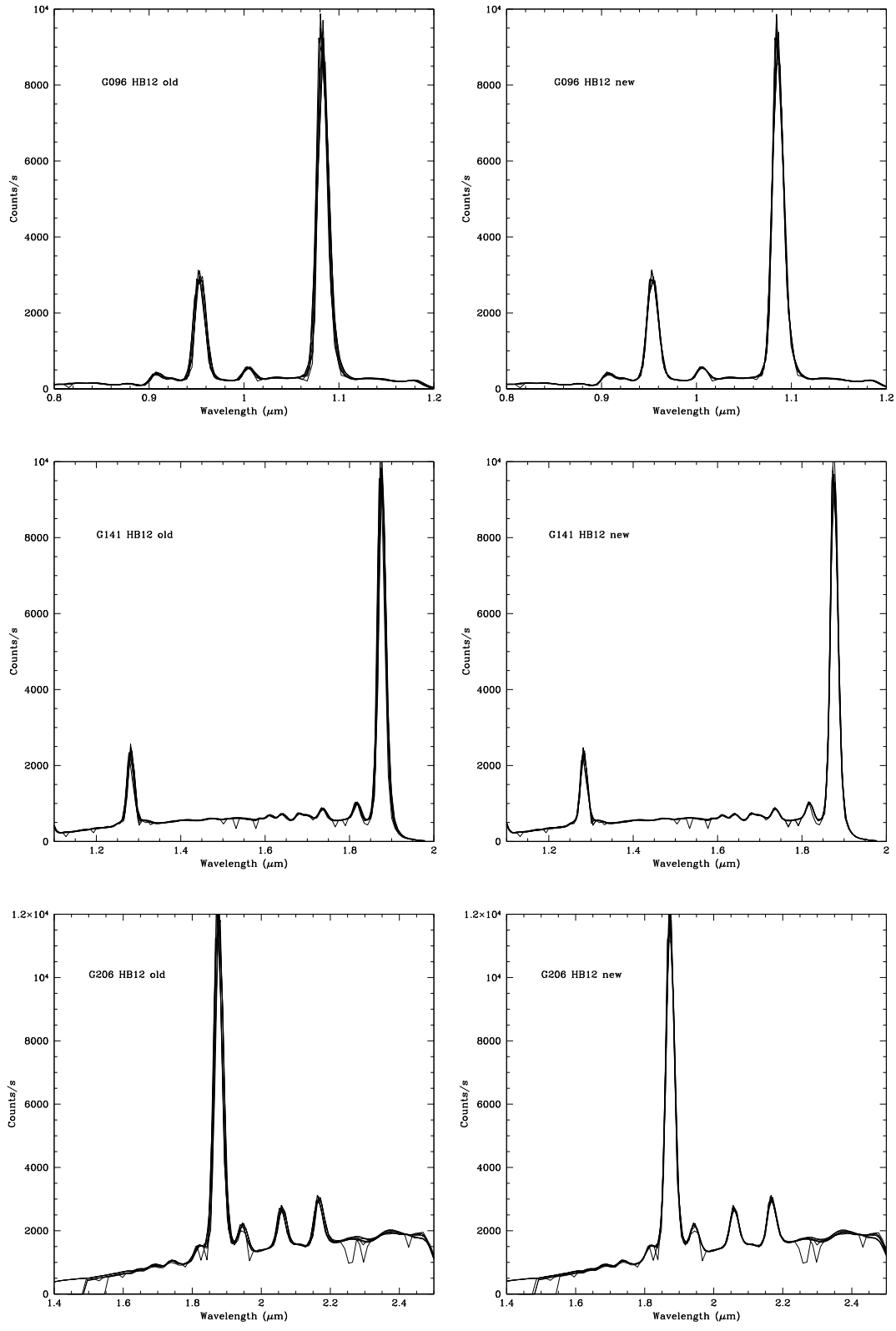

Figure 11: Closeup of emission features in the extracted spectra of HB12 in all three grisms. Left panels show the previous wavelength calibration and the right panel shows the results from this ISR.

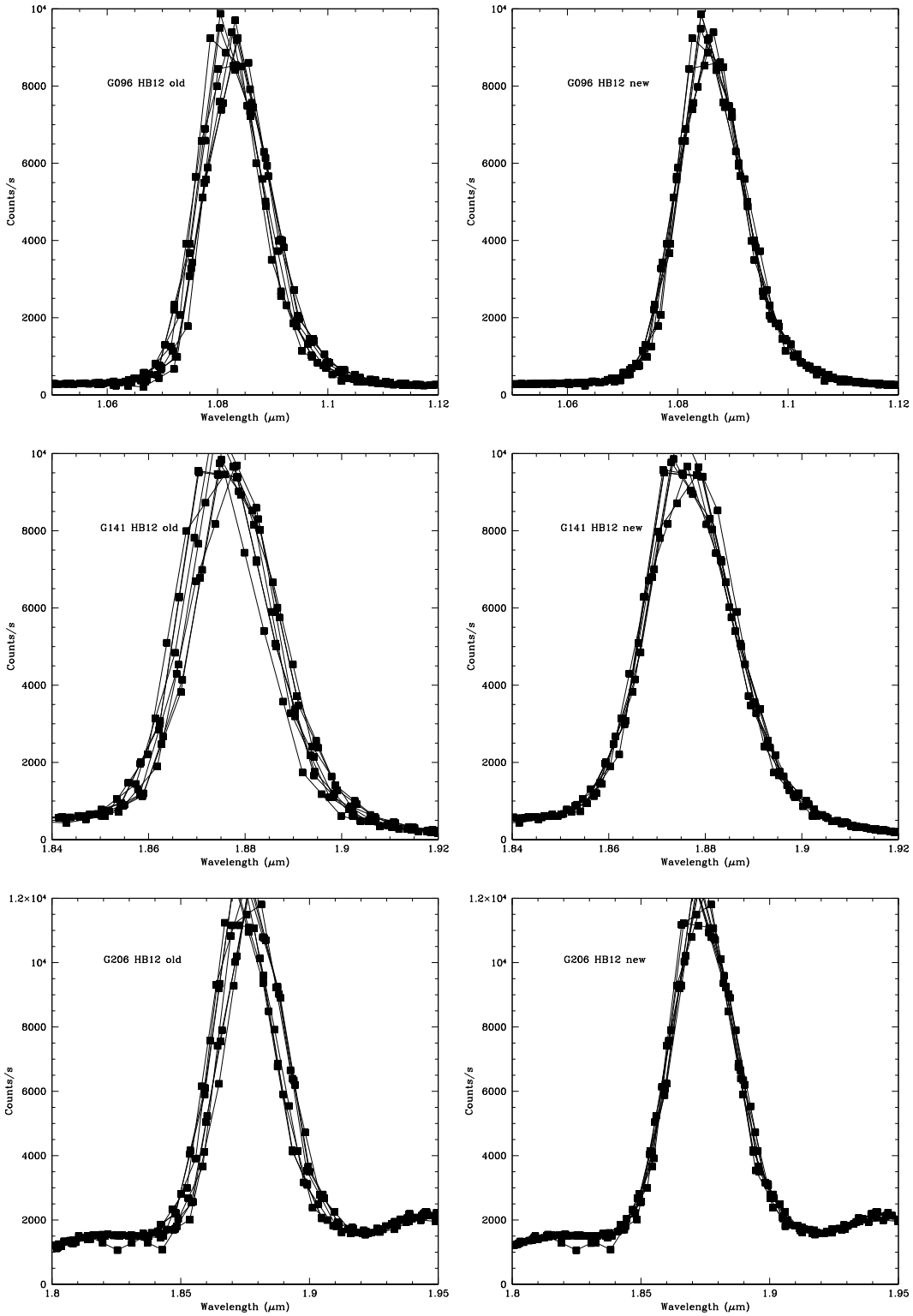

Conclusion

New Cycle 16 observations of two Planetary Nebulae, VY2-2 and HB12, were used to derive new wavelength calibrations of the G096, G141, and G206 grisms. These data were taken over a time span of 3 months and were taken in different corners on the detector in order to determine if the NICMOS grisms suffered from a significant amount as time variability as well as time variability.

Averaged-over-the-field values of the wavelength calibration that are within errors of the previously published values for all three grisms were derived. The small standard deviation of these measurements point to only a very small amount of field dependence, while no time dependence in those values was detected. The NICMOS grism has remained very stable over the course of several years.

Using the many dithered positions at which these objects were observed, the field dependence of the wavelength calibration of the NICMOS grisms was measured and calibrated. This field dependence is on the order of only 1-2% peak to peak. The parametrization of this field dependence was done in a manner that is directly useable by the slitless extraction software aXe.

References

Hora, J. and al., 1999, ApJS, 124, 195

Kümmel M, Walsh J.R., Pirzkal N., Kuntchner H., Pasquali A., 2009, PASP, 121, 875,99